Aberrant subcellular localization of mismatch repair protein MLH1 dysregulates the cell cycle to create new therapeutic opportunities

Mazumder A[1], DeWitt JT[1], Oropeza E[1], Punturi N[2,3], Lozano D[2,3], Sajjadi E[4,5], Guerini-Rocco E[4,5], Venetis K[4,5], Ivanova M[4], Mane E[4], Fusco N[4,5], Haricharan S[1,6].

Affiliations:

[1]San Diego State University Research Foundation, San Diego, CA

[2]Aging and Cancer Immunology, Sanford Burnham Prebys Medical Discovery Institute, La Jolla, CA

[3]NCI-designated Cancer Center, Sanford Burnham Prebys Medical Discovery Institute, La Jolla

[4]Division of Pathology, European Institute of Oncology IRCCS, Milan, Italy

[5]Department of Oncology and Hemato-Oncology, University of Milan, Milan, Italy

[6]Cancer Biology and Signaling Program, UCSD Moores Cancer Center, San Diego, CA

*Correspondence to be addressed to Svasti Haricharan (haricharans@sdsu.edu)

Abstract:

Mismatch repair loss is a commonly used prognostic and predictive clinical diagnostic across several cancer types. Currently, mismatch repair loss is assessed using bulk tumor approaches to assess genome instability (e.g. tumor mutation burden, microsatellite instability) or by immunohistochemistry for total protein level of individual mismatch repair proteins. Here, we identify a novel mechanism by which mismatch repair proteins are dysregulated that cannot be detected by either of these clinical diagnostic approaches. Sub-clonal mutations in *MLH1*, a principal mismatch repair gene, detected in tumors from estrogen receptor positive breast cancer patients do not impact abundance of MLH1 protein, nor do they contribute sufficiently to genomic instability to enable detection at the bulk tumor level. However, as we demonstrate here, some of these sub-clonal mutations aberrantly localize MLH1 protein to the cytoplasm, preventing MLH1-mediated activation of the G1 cell cycle checkpoint in response to standard targeted endocrine therapies. The lack of G1 checkpoint activity results in treatment resistance of a sub-clonal persister-like population that remains viable even after long-term exposure to treatment. The dependence on G1 progression, however, renders these sub-clonal populations acutely sensitive to CDK4/6 inhibitors such as palbociclib. Overall, data presented here strongly suggests that aberrant cytoplasmic localization of MLH1 can serve as a predictive biomarker to more accurately predict resistance to endocrine therapy, and sensitivity to combinatorial treatment with CDK4/6 inhibitors. This is particularly important in the adjuvant setting where the risk-benefit ratio for untargeted CDK4/6 inhibitor intervention is narrow. It is possible that these findings have important implications for treatment guidance in other non-breast cancer types as well, where *MLH1* mutation is even more frequent.

Introduction:

Mismatch repair (MMR) deficient tumors harbor defects in major genes of the DNA MMR system (MLH1, MSH2, MSH6, PMS2)[1], [2]. They display a molecular phenotype characterized by the genetic instability of numerous microsatellite repeat sequences throughout the genome referred to as MSI (for MicroSatellite Instability)[3]. MSI was first described in inherited tumors associated with Lynch syndrome. It has independent prognostic value in several primary tumors and can be associated with alternative response to standard of care. For instance, in colorectal cancer, DNA mismatch repair deficiency (dMMR) is a predictive marker for lack of efficacy of fluorouracil-based adjuvant therapy. For stage III patients with MSI/dMMR status, adjuvant chemotherapy with combination of oxaliplatin and fluoropyrimidines is given, while for non-MSI/MMR proficient elderly patients, oxaliplatin is not a standard treatment[4]. Additionally, for metastatic patients MSI status is routinely used biomarker to predict efficacy of immunotherapies including (anti-PD1, anti-PDL1 and anti-CTLA4)[3]. This finally led to approval of pembrolizumab and therefore, MSI status is now routinely tested for patients across a broad spectrum of cancers.

In context of hormone positive (HR+) breast cancer, the prognostic role of MMR deficiency has been confirmed by several studies, but its predictive value remains a matter of controversy[5]. HR+ breast cancer is more likely to have sporadic or somatic MMR loss, detectable in 10-15% of patients. Additionally, mutations in MMR genes are relatively rare in HR+ breast cancer, occurring in 1-3% of primary tumors, with the majority of MMR loss being achieved through downregulation of gene expression[6]. However, as we previously showed, MMR loss increases to ~30% in endocrine treatment resistant ER+ primary patient tumors, suggesting that MMR loss may be sub-clonal at initial diagnosis and therefore, difficult to assess with canonical clinical diagnostics[7]. Moreover, most mutations in MMR genes in

HR+ breast cancer are variants of unknown significance, and the phenotypic impact of these mutations in the context of cancer-relevant phenotypes remains uncertain.

Sub-clonal diversity is one of the key factors which contribute to endocrine treatment resistance in ER+ breast tumors[8], [9]. Indeed, many excellent studies of ER+ patient tumors in the literature demonstrate that acquired drug resistance is largely due to drug-refractory sub-populations (subclones) within these heterogeneous tumors[10], [11], [12], [13] . Subclones may remain unnoticeable for many years and ultimately expand resulting in treatment resistance and metastatic recurrence. Resistant subclones can be pre-existing (where they remain non-responsive to treatment early on) or acquired (where new aberrations are introduced partly due to the selective pressure of treatment)[14], [15], [16], [17], [18], [19].

For patients who relapse with endocrine resistant disease, CDK4/6 inhibitors such as palbociclib, ribociclib and abemaciclib have emerged as a handful of targeted agents approved in combination with endocrine therapy as front-line treatment[20]. Although the combination of CDK4/6 inhibitors and endocrine therapy improves median progression free survival, it does not prolong overall survival [20]. This is likely because many patients who initially benefit from CDK4/6 inhibitor treatment eventually develop resistance, while several studies suggest that a proportion of patients never benefit from this combination at all. Most successful targeted therapies have complementary diagnostic biomarkers to identify responsive patient populations[21]. There is no such clinically available biomarker for predicting response to CDK4/6 inhibitors. In this sense, CDK4/6 inhibitors have been identified as a targeted yet “biomarker-untargeted” therapy [19] . Therefore, there is an urgent and immediate need for complementary diagnostics to identify patients who are likely to respond well or who fail to respond to CDK4/6 inhibitors. We previously showed that loss of MLH1 can induce responsiveness to other non-endocrine targeted therapies including CDK4/6 inhibitors by dysregulating the cell cycle in ER+ breast cancer[7]. The characterization of MMR status in these patients

is troubled by the lack of tumor-specific guidelines and/or companion diagnostic tests. Using multiple model systems as well as data from clinical trials we present our observation with high clinical relevance showing cytoplasmic MLH1 may serve as a diagnostic candidate to predict response to CDK4/6 inhibition.

Material and Methods:

Cell lines, mice, si/shRNA transfection, and growth assays

Cell lines were obtained from ATCC (2015) and maintained and validated as previously reported. Mycoplasma tests were performed on parent cell lines and stable cell lines (latest test) with Lonza Mycoalert Plus Kit (Cat# LT07-710) as per the manufacturer's instructions. Transient transfection with mutant MLH1 constructs (purchased from TWIST Biosciences) and siRNA against CDK4/6 (purchased from Sigma-Aldrich) was conducted using JetPrime PolyPlus transfection reagent. Stable cell lines were maintained in the presence of specified antibiotics at recommended concentrations. Knockdown and expression was validated using western blotting. Growth assays were conducted using cytoSmart cell counter. Growth assay results were plotted as fold change normalized as specified. Three-dimensional growth assays were conducted over 6-8 weeks with twice weekly drug treatments using standard protocols. Images were captured when colonies were established and then treatment was administered, with images taken again every week. Fold change in area of colonies was calculated over time and represented as %growth. Tumor growth assays in vivo were carried out by injecting 5-7 x10^6 MCF7 cells into the L4 mammary fat pad/mouse. Mice for MCF7 experiments were 4-to-6-week athymic nu/nu female mice (from SBP animal facility). Tumors were randomized for treatment at ~100-150 mm^3 volume for MCF7 xenografts. Tumors were harvested at <2 cm diameter and were embedded in paraffin blocks, OCT and snap frozen. All mouse experiments were performed in compliance with all relevant ethical regulations for animal testing and research, and all experiments conducted in the study received approval from Sanford Burnham Prebys.

Inhibitors and Agonists

All drugs were maintained as stock solutions in DMSO, and stock solutions were stored at –80 and working stocks at –20 unless otherwise mentioned. 4-OHT (cat# H7904) and fulvestrant (cat# I4409) were purchased from Sigma-Aldrich, and stocks were diluted to 10 mmol/L working stocks for all experiments other than dose curves, where specified concentrations were used. For all experiments, cells were treated 24 hours after plating, and thereafter every 48 hours until completion of experiment. For mouse xenograft experiments, fulvestrant concentrations of 250 mg/kg body weight were used. Beta-estradiol was purchased from Sigma-Aldrich (cat# E8875), maintained in sterile, nuclease-free water, and diluted to obtain 10 mmol/L stocks for all experiments. For mouse xenograft experiments, 17 ß-estradiol was added to the drinking water twice a week at a final concentration of 8 µg/mL (cat# E2758; Sigma). CHK2 activator (3, 3;-diindolyl methane, cat# sc-204624; Santa Cruz Biotechnology) was used at 100 µmol/L concentrations. Abemaciclib (LY2835219, cat# S7158; SelleckChem) and palbociclib (PD-0332991, cat# S1116; SelleckChem) were used at 2.5 umol/L final concentrations for cell line assays and at 70 mg/kg/day in chow for tumor growth assays as described previously.

Flow cytometry, Immunostaining and Microscopy

Flow cytometry was conducted to determine differential growth effects caused by presence or absence of estrogen (E2) for cells harboring WT or mutant MLH1 when grown in co-culture. MCF7 cells with G55V mutation that were positive for GFP were plated at a 1:10 ratio with WT MLH1 MCF7 cells. Cells were analyzed at D0 and D7 post E2 or no E2 treatment. On D0 and D7 cells were trypsinized, washed and resuspended in 1X PBS + 2% FBS supplementation with DAPI as a viability marker and stored on ice until analyzed. GFP+ and GFP- populations of live cells were determined by flow cytometry using Aurora 5-laser Full Spectrum Analyzers (Aurora 5L).

Immunostaining was performed based on manufacturer's instructions. Cells were washed in 1X PBS; fixed for 20 minutes at room temperature in 4% PFA; blocked for 1 hour at room temperature in 5% goat serum and 1% Triton X-100 in 1x PBS; incubated with primary antibody overnight at 4 degrees in 1% goat serum and 1% Triton X-100 in 1x PBS antibody diluent; incubated with secondary antibody in diluent for 1 hour at RT; and then mounted with DAPI-containing mounting media (cat# P36935). Primary antibodies used include MLH1 (Cell Signaling Technology; cat# 4256; 1:200), pChek2 (cat# 2197), PCNA (cat# 2586) and Ki67 (cat# 9027). Fluorescent images were captured with an ECHO microscope and quantified with ImageJ.

qPCR and Western blotting

2×10^5cells were seeded overnight per well in 6-well plates. Following treatment with fulvestrant 1μM for 36 h, total RNA was extracted using RNeasy Mini Kit (Qiagen, Hilden, Germany). cDNA was synthesized using oligo(dT) and random primers (AB Bioscience, MA, USA), and qPCR analysis was performed with SYBR Green (Roche, NJ, USA). Primers for each were designed using NCBI primer blast and were ordered from Integrated DNA Technologies (IDT). 36B4 was used as internal control. Western blotting was conducted as previously described. All antibodies were purchased from Cell Signaling Technology and used at 1:1,000 dilutions unless otherwise specified. Primary antibodies were incubated with the membrane overnight at 4 degrees and included MLH1 (cat# M8320), CDK6 (cat# D48S8) and GAPDH (cat# 2175, 1:5,000).

3D spheroids and sub-clonal assays

For 3D spheroid assays, $4x10^3$ T47D cells were plated in 96 well-plate pre-coated with 1.5% agar. For sub-clonal 3D assay, G55V (GFP) and WT T47D cells were mixed in 1:9 ratio. Spheroids were allowed to grow for 1 week followed by respective treatments for 4 to 6 weeks. For -E2/+E2 experiments, 10nM of estradiol was added in the +E2 condition biweekly. For all other drug assays, fresh drug or vehicle were added biweekly. Spheroid pictures were captured using ECHO microscope and

quantification of size was done using image J software. For in vivo sub-clonal xenograft experiment, G55V (GFP) and WT MCF7 cells were mixed in 1:9 ratio. A total of 5x106 cells were injected into the left flank. Tumors were randomized for +E2 and -E2 group at ~100-150 mm3 volume. Tumor measurements were taken biweekly and bioluminescence pictures of mice were also captured using IVIS spectrum imaging system. Tumors were harvested at <2 cm diameter and were embedded in paraffin blocks, OCT and snap frozen.

PDxO establishment and treatments

For PDxO preparation, PDX tissue chunks were digested in a GentleMACS dissociator in warm advanced DMEM/F12 with GentleMACS human tumor dissociation enzymes and 10 µM Y-27632 added. After digestion, differential centrifugation was performed to enrich for organoids and deplete single cells. Organoids were embedded in 200-µl Matrigel domes, which were plated in six-well tissue culture plates onto a 50-µl Matrigel base layer. After a 5-min incubation period, plates were flipped, and Matrigel domes were solidified for 10 min before subtype-specific culture medium was added. For all breast cancer subtypes, 10 µM Y-27632 was added fresh to the PDxO base medium (Advanced DMEM/F12 with 5% FBS, 10 mM HEPES, 1× Glutamax, 1 µg ml–1 hydrocortisone, 50 µg ml–1 gentamicin and 10 ng ml–1 hEGF). Medium was exchanged every 3 to 4 d, and, once mature, cultures were passaged by incubating in dispase solution (20% FBS in dispase with Y-27632), followed by a wash step with base medium and a dissociation step in TrypLE Express. Single cells were seeded at 200,000–400,000 cells per dome. For drug treatments, Mature organoids were collected from culture using dispase treatment at 37 °C for 25 min. Five thousand to ten thousand cells (~50 organoids) were seeded per well in 96 tissue culture plates, each comprising a solidified 10-µl Matrigel base layer and 100 µl of PDxO medium supplemented with 5% (by volume) Matrigel. Media was replaced every 48 h with fresh drug. Cell titre glo 3D was conducted to measure viability.

Statistical analysis

Statistical significance between two groups was assessed by the unpaired Student's t-test. For spheroid experiments and tumor growth rates, slopes were calculated and compared for statistical differences. For categorical data, a Fisher's Exact or a Pearson's Chi-squared test was used as indicated based on sample size. All experiments were conducted in triplicate and each experiment was duplicated 2 or >2 times.

Results

MLH1 mutations cause varying degrees of endocrine treatment resistance in ER+/HER2 breast cancer cells.

We identified 6 somatic *MLH1* mutations from primary and metastatic patient tumor samples using three independent cohorts (NeoPalAna (primary), TCGA (primary) and MSKCC (primary and metastatic)). Three of the selected mutations were missense (G55V, E199K and D584H) and three nonsense (E414, E439 and E717) spanning the different protein-coding domains of *MLH1* (Fig 1A). We then transfected ER+/HER2- breast cancer cell lines (MCF7 and T47D) shRNA against *MLH1* with sh-resistant mutant and wildtype constructs. Protein levels of the missense mutated MLH1 constructs are comparable to that of wildtype constructs and to endogenous MLH1 levels, while nonsense mutated MLH1 constructs are analogous to shMLH1 untransfected cells in both transiently transfected (Fig S1A) and stably transfected (Fig 1B) cells. Next, we tested whether these selected MLH1 mutations alter response to endocrine therapy. We treated cell lines with either transient (Fig S1B) or stable (Fig 1C) expression of the six mutant constructs with the two of the common classes of endocrine therapy given to patients: fulvestrant (SERD) or tamoxifen (SERM) and assessed 2D growth. We observed no significant difference in baseline 2D growth rates for any of these mutations whether expressed in MCF7 (Fig S1C) or T47D (Fig S1D) cell line.

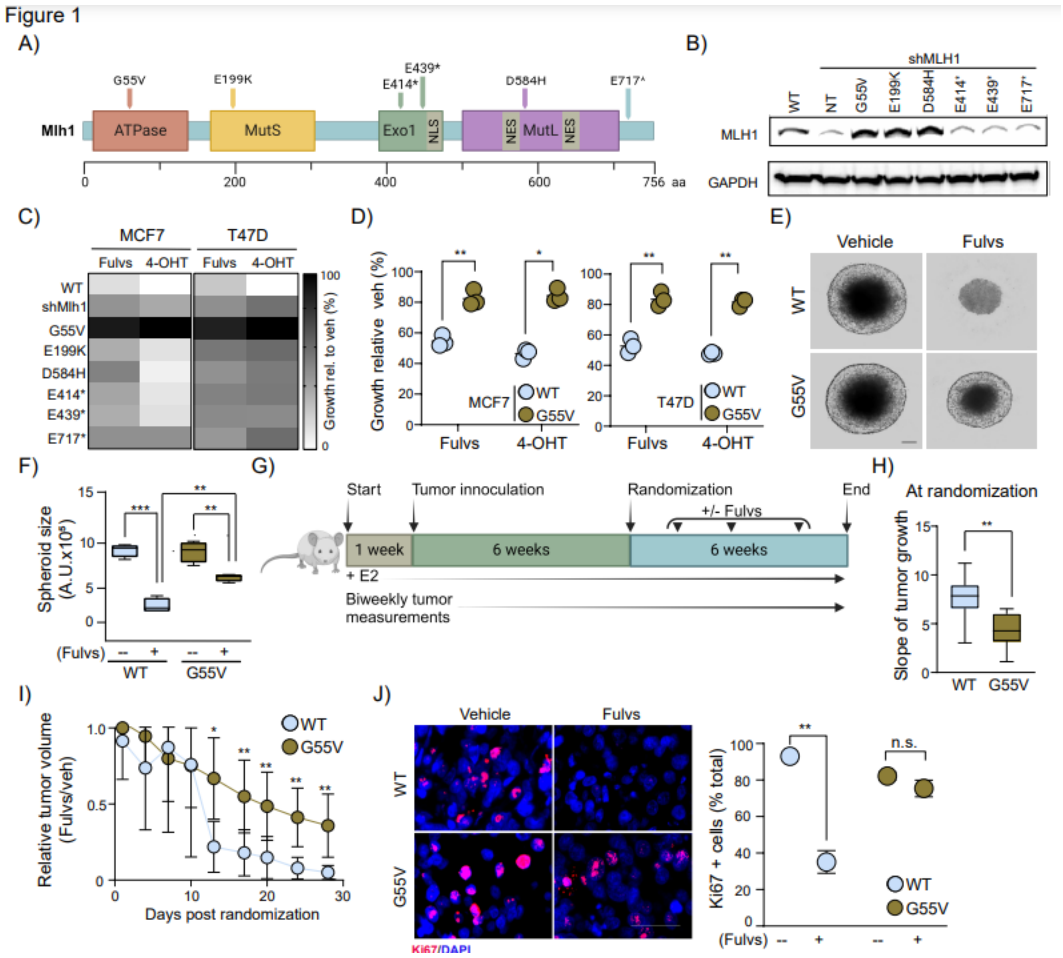

Figure 1: Some MLH1 mutations induce endocrine therapy resistance. (A) Schematic showing clinical mutations in the MLH1 gene . (B) Transient expression of sh-resistant mutants and wild type constructs in MCF7 cells stably expressing shRNA against MLH1. Associated data validating stable expression of mutant and wild type constructs in MCF7 cells presented in fig S1A. (C) Heatmap indicating growth expressed as % of vehicle for MCF7 and T47D cells transiently expressing mutants and wild type constructs after fulvestrant (100nM) or 4-OHT (100nM) treatment. Associated data validating endocrine therapy response in MCF7 and T47D cells stably expressing mutants and wild type constructs presented in fig S1B. (D) Graph depicting growth of MCF7 and T47D cells transiently expressing G55V mutant and WT construct after fulvestrant or 4-OHT treatment relative to vehicle. (E) Representative images of 3D growth assays of T47D spheroids stably expressing G55V mutant or WT construct after fulvestrant treatment. (F) Accompanying box plot with quantification. Associated data of 3D growth assay after tamoxifen (4-OHT) treatment fig S1E. (G) Schematic of in vivo experimental design. (H) Boxplots depicting differences in tumor growth rate at baseline before randomization (calculated as slope from growth curve of each tumor) of MCF7 cells stably expressing G55V mutant or WT construct. (I) Tumor volume normalized to

vehicle with biweekly administration of fulvestrant. (J) Representative images of ki67 staining (proliferation marker) in G55V or WT tumors with and without fulvestrant treatment with accompanied quantification. Student t-test was performed to determine all p values. ** represents p<0.005 and * p<0.05. For all graphs, error bars describe standard deviation. Scale bar = 20μM. Abbreviation Vehicle (Veh), Fulvestrant (Fulvs), Tamoxifen (4-OHT), Wild type (WT), not significant (n.s.)

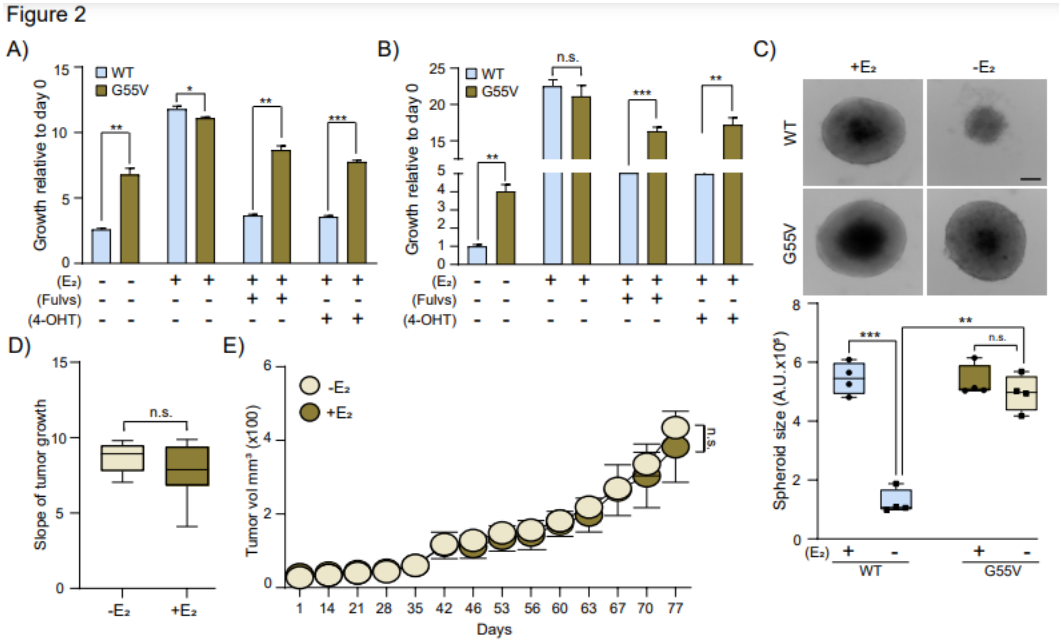

Figure 2: Some MLH1 mutations induce estrogen-independent growth of ER+ breast cancer cells. (A-B) Bar graph depicting growth of MCF7 cells (A) and T47D cells (B) stably expressing G55V mutant or WT constructs at day 7 relative to day 0 with or without addition of 10nM beta-estradiol to cells grown in charcoal stripped serum and treated with Fulvs (100nM) or 4-OHT (100nM) as indicated. (C) Representative pictures of 3D spheroids of T47D cells grown in charcoal stripped serum with (+E2) or without (-E2) 10nM beta-estradiol treatment. accompanying box plots showing quantification of spheroid size. (D) Boxplots depicting differences in tumor growth rate (calculated as slope from growth curve of each tumor) of MCF7 cells stably expressing G55V mutant grown with or without estrogen supplementation in drinking water. (E) Change in tumor volume over a period with or without estrogen supplementation . Student's ttest was performed to determine p value. *** represents p<0.0001. Abbreviations, estrogen (E2), Fulvestrant (Fulvs), Tamoxifen (4-OHT), Wild type (WT), Not significant (n.s.).

However, we observed varying levels of endocrine treatment resistant growth induced by distinct MLH1 mutations both after transient (Fig S1B) and stable (Fig 1C) expression. Of all the mutations, G55V most significantly induces resistance to endocrine treatment, even surpassing cells with stable knockdown of MLH1 (Fig 1C). G55V-bearing cells continue to grow at 85-90% efficiency even in presence of endocrine treatment compared to the ~50% growth efficiency of WT-bearing cells relative to vehicle treated counterparts ($p<0.05$) across all cell lines tested (Fig 1D).

Since the G55V mutation most strongly and consistently drives endocrine treatment resistant growth in independent cell lines, in response to different treatment modalities and when expressed either stably or transiently, we selected this mutation for further investigation. Using the cell lines with stable and robust expression of the G55V mutation construct (Fig 1B, S1A), we conducted 3D growth assays (Fig 1E). G55V-bearing spheroids retain ~60% 3D growth efficiency even after fulvestrant treatment compared to WT-bearing spheroids which fall to ~35% growth efficiency ($p=0.0004$) (Fig1E-F). These results are reproducible with tamoxifen treatment ($p=0.002$) (Fig S1E). To validate these findings *in vivo*, we xenografted mice with MCF7 shMLH1 cells stably expressing either G55V or WT MLH1 constructs (Fig 1G). We found that G55V tumors grow marginally slower than WT tumors in vehicle-treated mice ($p=0.0001$) (Fig 1H). However, even after 4 weeks of fulvestrant treatment, G55V-bearing tumors remain at 40% growth efficiency relative to vehicle-treated counterparts, unlike WT-bearing tumors, which show almost complete regression ($p=0.006$) (Fig 1I). In keeping with this increased resistance to fulvestrant *in vivo*, G55V-bearing tumors from fulvestrant-treated mice continue proliferating at the same rate as those from vehicle-treated mice, unlike WT-bearing tumors, which retain <40% of their proliferative capacity, as assessed by Ki67 positivity, (Fig 1J).

To test whether the endocrine treatment resistance induced by the G55V mutation is due to a loss of dependence on estrogen signaling as the primary mitogenic stimulus, we assayed growth in response to estrogen deprivation in serum-starved

conditions. In MCF7 cells, estrogen deprivation of WT *MLH1*-bearing populations decreases growth to 16% of that observed in estrogen-supplemented cells, compared to the 55% growth efficiency retained by G55V-bearing cells (Fig 2A, p=0.003). In T47D cells, similarly, estrogen deprivation decreases growth of WT-bearing cells to 4% of that seen in estrogen-supplemented counterparts, while G55V-bearing cells remain at 20% growth efficiency (Fig 2B, p=0.003). This decreased dependence on estrogen as a primary mitogenic stimulus is even more pronounced in 3D growth assays where estrogen deprivation has little to no detectable impact on G55V-bearing spheroids while WT spheroids decrease dramatically to ~16% of the size of estrogen-supplemented controls (Fig 2C, p=0.0001). These observations validate *in vivo*: in MCF7 xenograft experiments, estrogen deprivation is unable to inhibit growth of G55V-bearing tumors (Fig 2D-E). Together, these findings support a causal role for the G55V mutation in endocrine treatment resistant growth despite robust and stable expression of the mutant MLH1 protein.

Sub-clonal mutation-bearing cells constitute an endocrine treatment resistant population.

We identified the G55V mutation in a primary ER+/HER2- breast cancer patient sample at a low variant allele frequency (VAF) of 3.38 (Fig 3A). After treatment with anastrozole (an aromatase inhibitor, with a similar mechanism of action to estrogen deprivation studies described above) for 28 days, this patient showed significant responsiveness to her treatment with a 62% decrease in proliferating cells (assessed using immunohistochemistry for proliferation marker Ki67in diagnostic and surgical biopsies). This response is comparable to that of other patients in the trial whose tumors had no detectable mutations in *MLH1* (Fig 3A). Since we observed significant induction of estrogen independent growth both *in vitro* and *in vivo* in ER+/HER2- breast cancer cells expressing G55V, we next asked whether sub-clonal populations of G55V-bearing cells, as in the patient tumor, remain resistant to endocrine interventions (Fig 3B). We designed experimental models that mimic the sub-clonal state observed in the patient tumor by admixing

WT and G55V-bearing isogenic cells in a 9:1 ratio. After a week of estrogen deprivation, flow cytometry assays in 2D growth models showed a significant (~40%) increase in the proportion of G55V cells in the estrogen-deprived condition (Fig 3C). We confirmed these findings by performing orthogonal 2D growth assays in both MCF7 and T47D cells where we immunohistochemically quantified WT- and G55V-bearing cell populations over 8 days of growth in response to estrogen deprivation. Similarly to the FACS experiment, G55V-bearing cells are enriched from 10% to 40% in the estrogen-deprived group relative to the estrogen-supplemented vehicle control (Fig 3D, $p=0.004$ (MCF7) $p=0.0002$ (T47D)). These data suggests that G55V-bearing cells have little or no growth advantage intrinsically but assume an adaptive growth advantage when cells are exposed to endocrine interventions. We confirmed these observations in response to fulvestrant (MCF7: Fig S2A, T47D: Fig S2C) and tamoxifen (MCF7: Fig S2B, T47D: Fig S2D) treatment in 2D growth assays. These findings also validate in 3D growth assays. After 6 weeks of estrogen deprivation, the proportion of G55V cells doubles ($p=0.01$) in estrogen-deprived conditions while remaining constant in the estrogen-supplemented controls (Fig 3E-F). Similarly, the G55V proportion increases 2-fold with fulvestrant ($p<0.0001$) (Fig S2E) and 3-fold with tamoxifen ($p<0.0001$) (Fig S2F) treatment, relative to vehicle controls. We then designed an *in vivo* subclonal competition assay by xenografting mixed population of G55V:WT -bearing MCF7 cells at a 1:9 ratio to form tumors in nude mice with estrogen supplementation (Fig 3G). As expected, when mice were randomized to estrogen-deprived or continued estrogen supplementation treatment arms, we saw a significant decrease in overall tumor volume ($p=0.014$) after estrogen deprivation (Fig 3G). However, the proportion of G55V-bearing cells (assessed by immunohistochemically detecting the GFP tag of G55V cells) increases to constitute almost 100% of the tumor area in the estrogen deprived mice, while remaining at ~20% tumor area in the estrogen supplemented control arm (Fig 3H, $p<0.0001$).

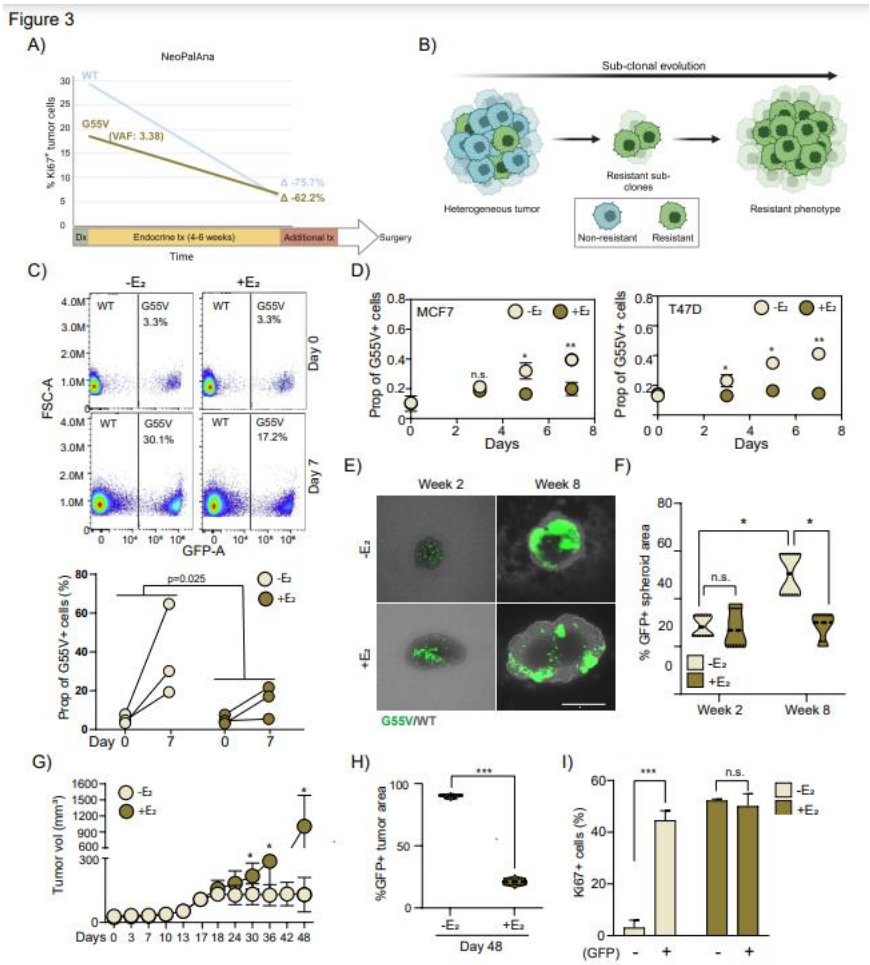

Figure 3: G55V mutation bearing cells persist in subclonal fractions even after administration of endocrine therapy. (A) Schematic from NeoPalAna trial, showing low variant allele frequency of G55V mutation in the patient and therefore, drop in Ki67 staining after initial endocrine therapy which is comparable to patients with WT MLH1. (B) Schematic showing evolution of sub-clonal resistant phenotype after endocrine intervention (C) Representative image from flow cytometry assays where MCF7 cells with G55V mutant (GFP+ cells) and WT cells mixed in 1:9 ratio were grown with or without 10nM of beta-estradiol for a week. The proportion of GFP positive cells were quantified on day 0 and day 7 in both -E2 and +E2 condition. Accompanied quantification. (D) Dot plots confirming in both MCF7 and T47D cells as indicated increase in GFP+ G55V cells independent of endocrine intervention. Associated data showing response to fulvestrant and tamoxifen presented in S2 A-D. (E) 3D spheroids of T47D cells with mixed population of G55V (GFP+) and WT constructs in (1:9) ratio grown with or without 10nM of beta-estradiol for 8 weeks. Green shows GFP+ G55V positive spheroid area. Accompanying quantification presented as violin plot. (F) Associated data showing response of fulvestrant and tamoxifen in 3D is presented in fig S2 E-F. (G) Change in tumor growth of MCF7 cells stably expressing G55V mutant (GFP+) and WT constructs mixed in 10:90

ratio grown with or without estrogen supplementation in drinking water. (H) Proportion of G55V (GFP+) tumor in both -E2 and +E2 condition at the end of experiment. (I) Quantification for Ki67+/GFP+/-(G55V) cells in both +E2 and -E2 condition. Accompanying representative pictures presented in fig S3B. Student's t test were performed to determine all p values. *** represents $p<0.0001$, ** $p<0.005$ and * $p<0.05$. For all graphs, error bars describe standard deviation. Scale bar = 50μM. Abbreviations, estrogen (E2), Wild type (WT), not significant (n.s.).

These observations are supported by assessment of proliferation in the tumors, where G55V-bearing tumor cells maintain their proliferative rate unperturbed even with estrogen deprivation, while the WT-bearing counterparts within the same tumor exhibit significant inhibition of proliferation (Fig 3I, S3B). These findings together suggest that in patient tumors, cells which carry G55V mutation may escape endocrine intervention when used as a first-line monotherapy. Because they are sub-clonal, however, they likely remain undetected precluding identification of these seeds of recurrence.

The G55V mutation mutes CHK2 activation leading to endocrine therapy resistance.

To identify the mechanism by which the G55V mutation confers resistance to endocrine treatment, we conducted RNAseq analysis of G55V- and WT-bearing isogenic MCF7 cells at baseline and after fulvestrant treatment. A reactome pathway analysis identified cell cycle dysregulation as one of the pathways distinguishing the G55V-bearing cellular response to fulvestrant from that of WT-bearing cells (FDR<0.05; Fig 4A, S4A). Specifically, genes involved in G1/S checkpoint activity are differentially regulated in G55V cells following fulvestrant treatment compared to both WT-bearing cells and isogenic cells expressing E717*, another *MLH1* mutation identified in patient tumors (Fig 4A). Chk2,a key G1 checkpoint kinase, constituted one of the top cell cycle regulators downregulated in G55V relative to control cells (Fig 4A). To validate this RNAseq observation, we tested Chk2 expression in our different experimental model systems. While more than 25% of MCF7 cells bearing WT *MLH1* have detectable pChk2 levels upon fulvestrant treatment, those with the G55V mutation have almost no detectable

Chk2 activation (p=0.004) (MCF7: Fig 4B; T47D: Fig S4B). Since Chk2 activation is known to arrest G1-S transition when ER+ breast cancer cells are exposed to endocrine therapy resulting in a proliferative block, we also assessed expression of S phase marker PCNA in our G55V and WT-bearing xenograft tumors. WT-bearing tumors have 75% decrease in S-phase cells in response to fulvestrant treatment,

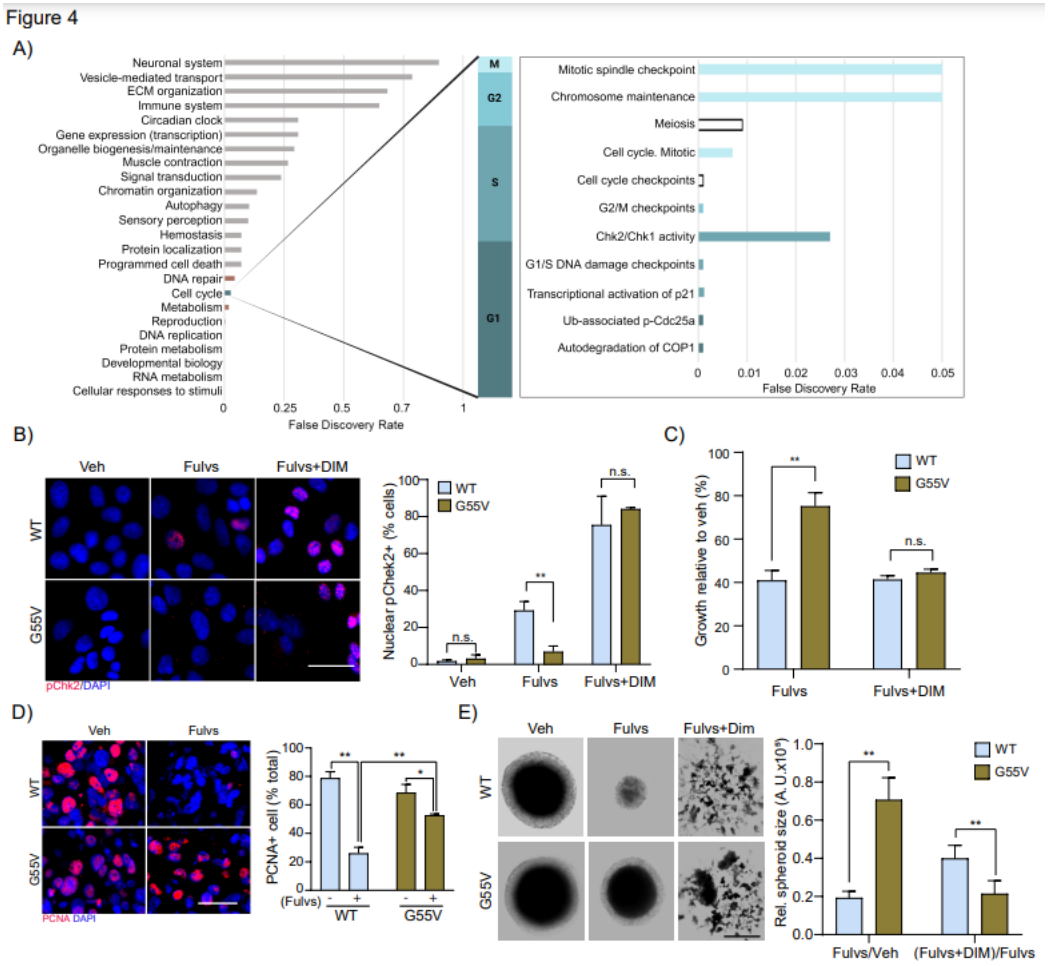

Figure 4: G55V prevents Chk2 activation despite abundant levels of MLH1 proteins. (A) Gene set enrichment analysis of RNAseq data comparing MCF7 cells with WT and G55V MLH1 constructs after treatment with fulvestrant 1uM for 36h. Enrichment of cell cycle checkpoint kinase activity. (B) Representative immunofluorescence pictures showing pChek2 expression in MCF7 cells with WT or G55V MLH1 constructs with or without treatment with fulvestrant 1μM or fulvestrant (100nM) + DIM (200μM) treatment for 36 h.Accompanied quantification presented as bar graph. . Associated data showing pChek2 expression in T47D cells presented in fig S4B,C. (C) Bar graph showing growth of MCF7 cells with G55V or WT MLH1 constructs after fulvestrant 1uM treatment for 36 h or fulvestrant (100nM) + DIM (200μM) treatment for 36 h. Growth is normalized to vehicle for each

type and expressed as percent inhibition. Associated data showing response in T47D cells is presented in fig S4D. (D) Representative immunofluorescence pictures showing PCNA expression in MCF7 xenograft tumors with WT or G55V MLH1 constructs with and without fulvestrant treatment. Accompanying quantification is shown as bar graph (E) Representative pictures of 3D spheroids of T47D cells with WT or G55V MLH1 constructs after biweekly treatment with fulvestrant 10nM or fulvestrant+Dim (10nM+50uM). Accompanied by quantification. Spheroid size was measured using Image J. Student's t-test was performed to determine all p values. ** represents $p<0.005$ and * $p<0.05$. For all graphs, error bars describe standard deviation. Scale bar = 50μM.Abbreviations, Vehicle (Veh), Fulvestrant (Fulvs), 3,3′-Diindolylmethane (DIM) chek2 activator.

while G55V-bearing tumors have a modest 24% decrease (Fig 4D). This striking discrepancy in Chk2- and associated G1 blockade suggests that impaired Chk2 activation in G55V tumors leading to a failed G1-S checkpoint block in response to endocrine treatment results in uncontrolled proliferation and treatment resistance.

To test this hypothesis functionally, we used the small molecule Chk2 activator, di-indolyl methane (DIM) to test whether Chk2 can be exogenously activated in G55V-bearing cells. DIM-treatment of G55V-bearing cells, unlike fulvestrant treatment, induces robust Chk2 activation comparable to that of fulvestrant-dependent activation of Chk2 in WT counterparts (MCF7: Fig 4B; T47D: Fig S4C). In validation of our hypothesis that loss of Chk2 activation in response to endocrine treatment in G55V-bearing cells mediates their resistance phenotype, administration of DIM rescued sensitivity to fulvestrant in G55V-bearing cells in 2D growth assays (MCF7: Fig 4C, T47D: Fig S4D). This Chk2 dependency validates in 3D spheroid assays where addition of DIM to fulvestrant, decreases spheroid size of G55V-bearing cells by 70% when compared to fulvestrant alone, phenocopying the effect of fulvestrant on WT-bearing cells ($p=0.0003$) (Fig 4E).

Aberrant subcellular localization of MLH1 dampens Chk2 activation in response to treatment.

MLH1 promotes Chk2 activation by binding to its upstream activator ATM and stabilizing it. Therefore, loss of MLH1 protein mutes Chk2 activation, an event

critical for mounting a cell cycle arrest response to the administration of endocrine treatment. However, the G55V mutant MLH1 protein is abundantly expressed in ER+/HER2- breast cancer cells (Fig 1B, Fig S1A) as detected by western blotting, suggesting that the loss of Chk2 activation in G55V-bearing cells is not due to destabilization of the MLH1 protein. Therefore, we next assessed the subcellular localization of the G55V mutant protein using immunofluorescence. While the number of ER+/HER2- breast cancer cells with nuclear WT MLH1 increases by 50% upon administration of endocrine treatment as previously reported (p=0.0003), cells expressing the G55V mutant protein show no detectable nuclear translocation and remain exclusively cytoplasmic both before and after endocrine treatment (Fig 5A, S5). The complete lack of nuclear presence of the G55V mutant MLH1 protein persists *in vivo* in xenograft tumors in contrast to isogenic tumors with WT MLH1 (p=0.009) (Fig 5B). The loss of cytoplasmic localization, therefore, likely phenocopies the effect of complete MLH1 loss on Chk2 activation. To test this hypothesis, we investigated whether cytoplasmic localization of MLH1, independent of a G55V mutation, also precludes Chk2 activation to drive endocrine treatment resistance.

To test this hypothesis, we screened panels of ER+/HER2- breast cancer PDXs from three collections (Huntsman Cancer Institute (HCI), Baylor College of Medicine (BCM) and Xenostart) for subcellular localization of MLH1 and pChk2 using immunofluorescence. In our first analysis combining HCI and BCM panels (n=4 HCI; n=6 BCM), we conducted an agnostic regression analysis between percentage of cells with cytoplasmic (but no nuclear) MLH1 and percentage of cells with pChk2 in each PDX tumor. We found significant inverse correlation between percentage of cells with cytoplasmic (and no nuclear) MLH1 and Chk2 activation (R^2=0.8829; p=0.0003) (Fig 5C with representative images from HCI: Fig S6A and BCM: Fig S6B panels). Then, using a third independent ER+/HER2- PDX panel (Xenostart, n=16), we categorized tumors as either cytoplasmic (<5% nuclear positive cells) or nuclear (>5% nuclear positive cells) for MLH1.

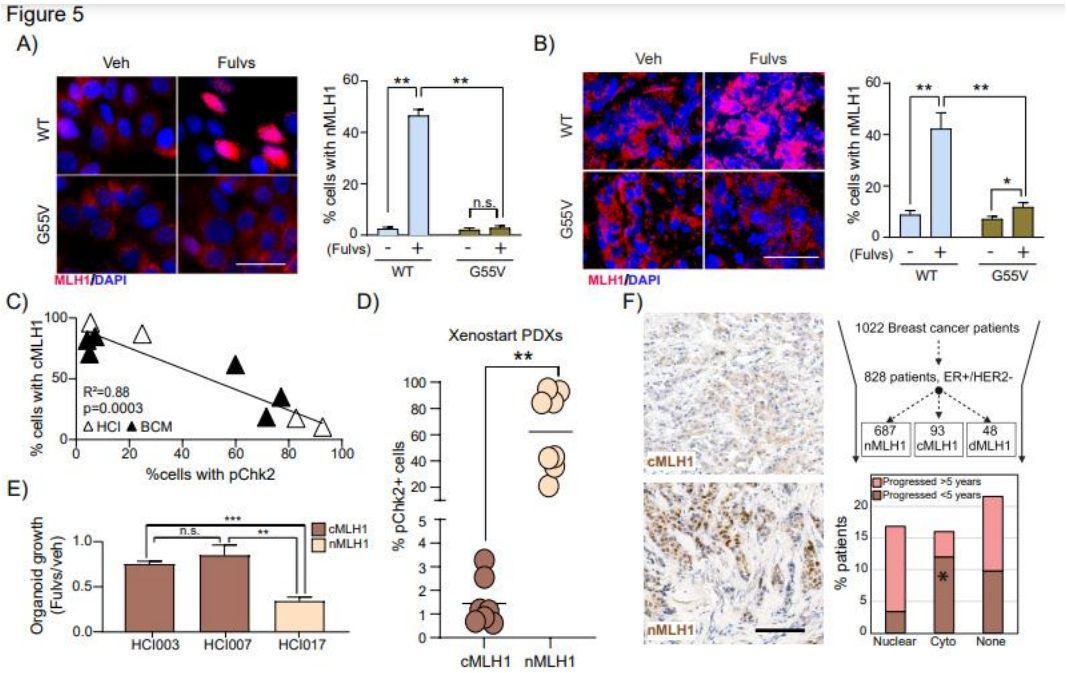

Figure 5: G55V alters subcellular localization of MLH1. (A) Representative immunofluorescence pictures showing subcellular expression of MLH1 in MCF7 cells with G55V or WT MLH1 constructs after fulvestrant 1uM treatment for 36 h. Accompanying bar graph showing quantification. Associated data for subcellular expression MLH1 in T47D cells is presented in fig S5. (B) Representative immunofluorescence pictures showing subcellular expression of MLH1 in MCF7 xenograft tumors with WT or G55V MLH1 constructs after fulvestrant treatment. Accompanying bar graph showing quantification. (C) Regression analysis showing association between cytoplasmic expression of MLH1 and and nuclear pChek2 in HCI and BCM PDX lines. (D) Dot plot represents association between cytoplasmic vs nuclear MLH1 with nuclear pChek2 expression in Xenostart PDX lines. Each dot represents and individual PDX line. Associated representative pictures of MLH1 and pChek2 expression for all PDXs is presented in fig S6A-C. (E) Bar graph showing effect of fulvestrant treatment in three PDX derived organoids (PDoX) models. 3D cell-titre glo was performed to measure viability. Growth is expressed relative to vehicle (DMSO treatment) for each PDoX. Student's t test was performed to determine all p values. *** represents $p<0.0001$, ** $p<0.005$ and * $p<0.05$. For all graphs, error bars describe standard deviation. Scale bar = 50μM (F)) Categorial analysis performed on MSKCC patient data showing patients with cytoplasmic MLH1 have a significant increase in progression of disease within 5 years which is least for patients with nuclear MLH1. Abbreviations, Vehicle (Veh), Fulvestrant (Fulvs), Wild type (WT), Hutchinson Cancer Institute PDXs (HCIs), Baylor College of Medicine PDXs (BCMs), Not significant (n.s.) and cMLH1 (cytoplasmic MLH1), nMLH1 (nuclear MLH1).

We found that PDX tumors that have nuclear MLH1 have ~60% positivity for nuclear pChk2, while those with cytoplasmic MLH1 show <2% positivity for nuclear pChk2 (Fig 5D, representative images in Fig S6C). To test whether this decrease in Chk2 activation in tumors with cytoplasmic MLH1 impacts the ability of tumors to resist endocrine treatment, we conducted *ex vivo* PDX organoid growth assays in the presence or absence of endocrine therapy. Both HCI003 and HCI007 PDX lines with cytoplasmic (and not nuclear) MLH1 are resistant to endocrine therapy, showing <25% growth inhibition, whereas organoids of HCI017 (with nuclear MLH1) show strong responsiveness with >75% growth inhibition after endocrine treatment (p=0.005) (Fig 5E).

To test whether these associations between cytoplasmic MLH1 and endocrine therapy resistance is detectable in patient tumors, we analyzed MLH1 subcellular localization and disease progression in a cohort of 828 ER+/HER2- breast cancer patients (Fig S7A). The biopsies were pathologically graded for cytoplasmic vs nuclear MLH1 on a scale of 0 to 3; where a score of 0 represents no cytoplasmic MLH1 whereas a score of 3 reflects >90% of cells with cytoplasmic MLH1. Tumors with neither cytoplasmic nor nuclear MLH1 presence were deemed deficient for MLH1. In this dataset, ~12% of ER+/HER2- breast cancer patient tumors had cytoplasmic MLH1, while ~5% were deficient for MLH1 (Fig S7B). Amongst the different tumor types, ER+/HER2- patient tumors were three times as likely to have high levels of cytoplasmic MLH1 as either HER2+ or triple negative tumors (Fig S7C-E). Cytoplasmic MLH1 presence in ER+/HER2- breast cancer patient tumors correlated with decreased time to progression (p=0.03), with 12% of patients with cytoplasmic MLH1 presence progressing within 5 years of diagnosis compared to only 2% of patients with nuclear MLH1 (Fig 5F). This increased immediate progression on first-line therapies is similar to that observed in patients deficient for MLH1 (Fig 5F). Together these data strongly support a role for cytoplasmic MLH1 in predicting cell cycle dysregulation that precludes response to standard endocrine therapies in ER+/HER2- breast cancer patients.

Cytoplasmic MLH1 induces CDK4/6 dependence in ER+/HER2 negative breast cancer cells.

Since ER+/HER2- breast cancer cells with cytoplasmic MLH1 fail to activate G1 checkpoint kinase Chk2 in response to endocrine treatment, unlike their counterparts with robust nuclear translocation of LMH1 (Fig 6A), we next tested whether aberrant cytoplasmic localization of MLH1 alters other key G1/S-phase cell cycle regulators. We found that G55V-bearing ER+/HER2- breast cancer cells, used here to represent cells with aberrant cytoplasmic MLH1 localization, increase levels of the G1 cyclin-dependent kinase CDK6 >2-fold, and the early G1 cyclin, CCND1 2-fold, upon endocrine treatment ($p=0.012$) when compared to cells bearing the WT (nuclear) MLH1 (Fig 6B). In further support of a role for cytoplasmic MLH1 localization in G1 dysregulation, G55V-bearing cells also downregulate p27, the G1 inhibitor that works directly downstream of Chk2 relative to WT-bearing cells (Fig 6B). To test whether upregulation of G1 CDKs by cytoplasmic localization of MLH1 induces cellular dependence on these CDKs for endocrine therapy resistant growth, we knocked down *CDK6* in MCF7 and T47D cells bearing G55V MLH1 using siRNA (Fig S8A). Knocking down CDK6 restores sensitivity to endocrine treatment in G55V-bearing isogenic counterparts of both MCF7 and T47D cells (MCF7: Fig 6C, T47D: Fig S8B). These data suggest that aberrant cytoplasmic localization of MLH1 induces dependence on G1 CDKs for endocrine therapy resistance in ER+/HER2- breast cancer cells invoking a potential therapeutic strategy in the form of CDK4/6 inhibitors. Both MCF7 and T47D cells with the G55V mutation have 30-50% growth inhibition after administration of CDK4/6 inhibitor palbociclib (MCF7: Fig 6D, T47D: Fig S8C) and abemaciclib (MCF7: Fig S8D, T47D: FigSE) in contrast to their counterparts with WT MLH1 which show no growth inhibition at all ($p<0.0001$). These results validate in 3D spheroid assays where G55V-bearing cells are significantly ($p<0.0001$) more susceptible to palbociclib treatment than WT-bearing cells (Fig 6E).

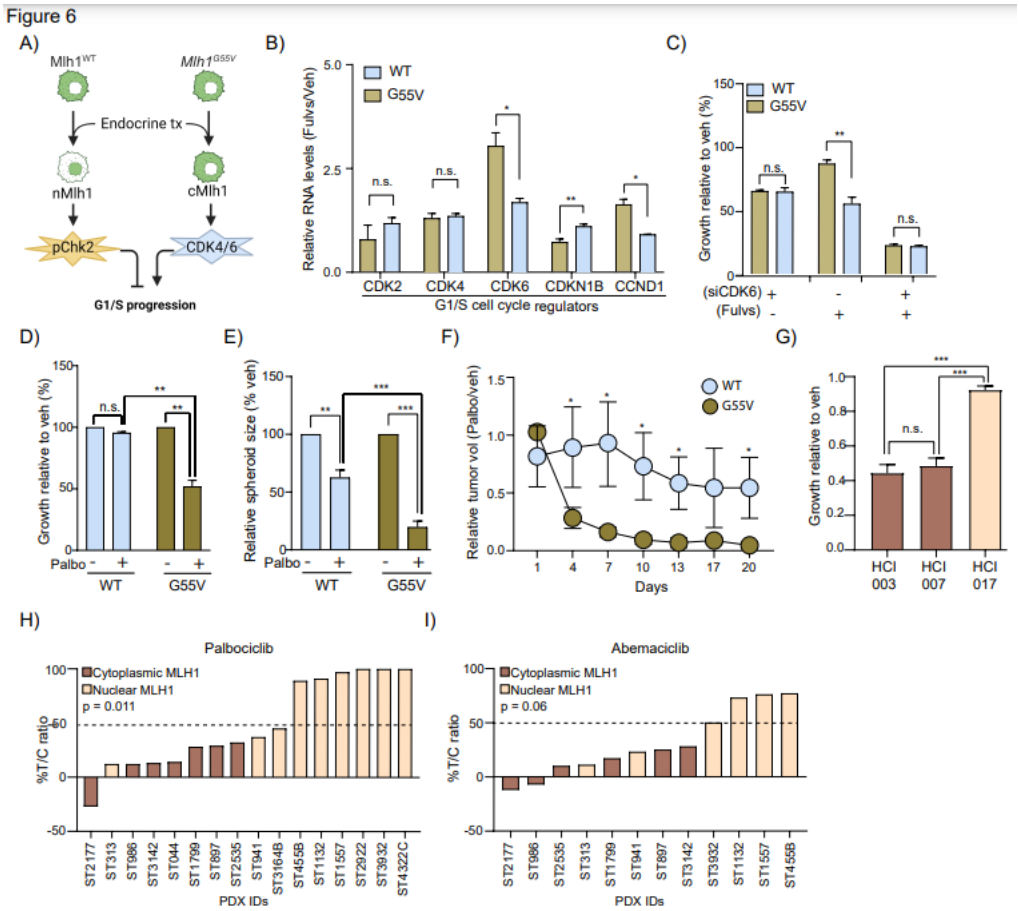

Figure 6: Cytoplasmic MLH1 predisposes sensitivity to CDK4/6 inhibition (A) Schema showing association between cytoplasmic MLH1 that results into impaired Chk2 activation and its effect on CDK activity. (B) RT-qPCR analysis of MCF7 cells for relative expression of indicated transcripts following fulvestrant treatment. (C) Bar graph showing growth of MCF7 cells with G55V or WT MLH1 constructs after siCDK6 knockdown alone or with fulvestrant treatment. Associated data validating knockdowns and growth in T47D cells in Fig S8 A, B. (D) Bar graph showing growth of MCF7 cells with G55V or WT MLH1 constructs after CDK4/6 inhibitor palbociclib treatment. Associated data for T47D cells in Fig S8C. (E) 3D growth of T47D cells harboring G55V or WT MLH1 after palbociclib treatment. (F) In vivo tumor growth expressed as change in tumor volume of MCF7 cells stably expressing G55V mutant and WT constructs after palbociclib treatment normalized to vehicle. Associated data showing tumor growth in vehicle and palbociclib is presented in Fig S8 F-G. (G) Bar graph showing effect of palbociclib treatment in three PDX derived organoids (PDoX) models. 3D cell-titre glo was performed to measure viability. Growth is expressed relative to vehicle (ultrapure water treatment) for each PDoX. (H-I) CDK4/6 inhibitor response expressed as percent Treatment/ Control ratio in PDX lines with cytoplasmic or nuclear MLH1 (H) Palbociclib (I) Abemaciclib. Student's t test was performed to determine all p values. For panel H and I Fisher's

exact test was performed to calculate p values. *** represents $p<0.0001$, ** $p<0.005$ and * $p<0.05$. For all graphs, error bars describe standard deviation.

Lastly, *in vivo,* G55V-bearing MCF7 xenograft tumors regress in response to monotherapy with palbociclib, showing significant inhibition in tumor growth compared to WT-bearing tumors ($p=0.032$), (Fig 6F, tumor volumes for vehicle-treated mice in Fig S8F and for palbociclib-treated mice in Fig S8G).

Next, we tested whether susceptibility to CDK4/6 inhibitors extend to non-mutational cytoplasmic MLH1 localization, by assessing *ex vivo* growth response in the HCI PDX panel. Both HCI003 and HCI007 (with cytoplasmic MLH1) have >50% growth inhibition after palbociclib treatment ($p<0.0001$) while HCI017 (with nuclear MLH1) shows <10% growth inhibition with this monotherapy (Fig 6G). Similarly, *ex vivo* growth in the Xenostart PDX panel indicates enrichment for palbociclib (Fig 6H, $p=0.01$) and abemaciclib (Fig 6I, $p=0.06$) responders in tumors with substantive cytoplasmic (and not nuclear) MLH1 presence. To test whether this casual link between cytoplasmic MLH1 and CDK4/6 sensitivity extends to patients, we investigated the correlation between sub-clonal MLH1 mutations and treatment response in two independent clinical trials. In the NeoPal Ana trial (Fig 7A), we identified two patient tumors of interest: one with G55V mutation (3% VAG) and another with G47C mutation in the same ATPase domain of MLH1 gene as G55V. While these tumors appear responsive to initial endocrine treatment in terms of bulk proliferative inhibition as measured by Ki67 positivity, both tumors show significant further inhibition in proliferation after palbociclib treatment (80% and 84% growth inhibition, respectively; Fig 7B). This is in sharp contrast to patient tumors with WT MLH1 who demonstrate 70% growth inhibition with endocrine treatment alone and no further proliferative inhibition with the addition of palbociclib (Fig 7B). In a second clinical trial, NCT3007979 where circulating tumor DNA (ctDNA) was analyzed at baseline and serial time points after cyclical CDK4/6 inhibitor treatment to evaluate genomic alterations, mutational signatures, and blood tumor mutational burden (bTMB) (Fig 7C),

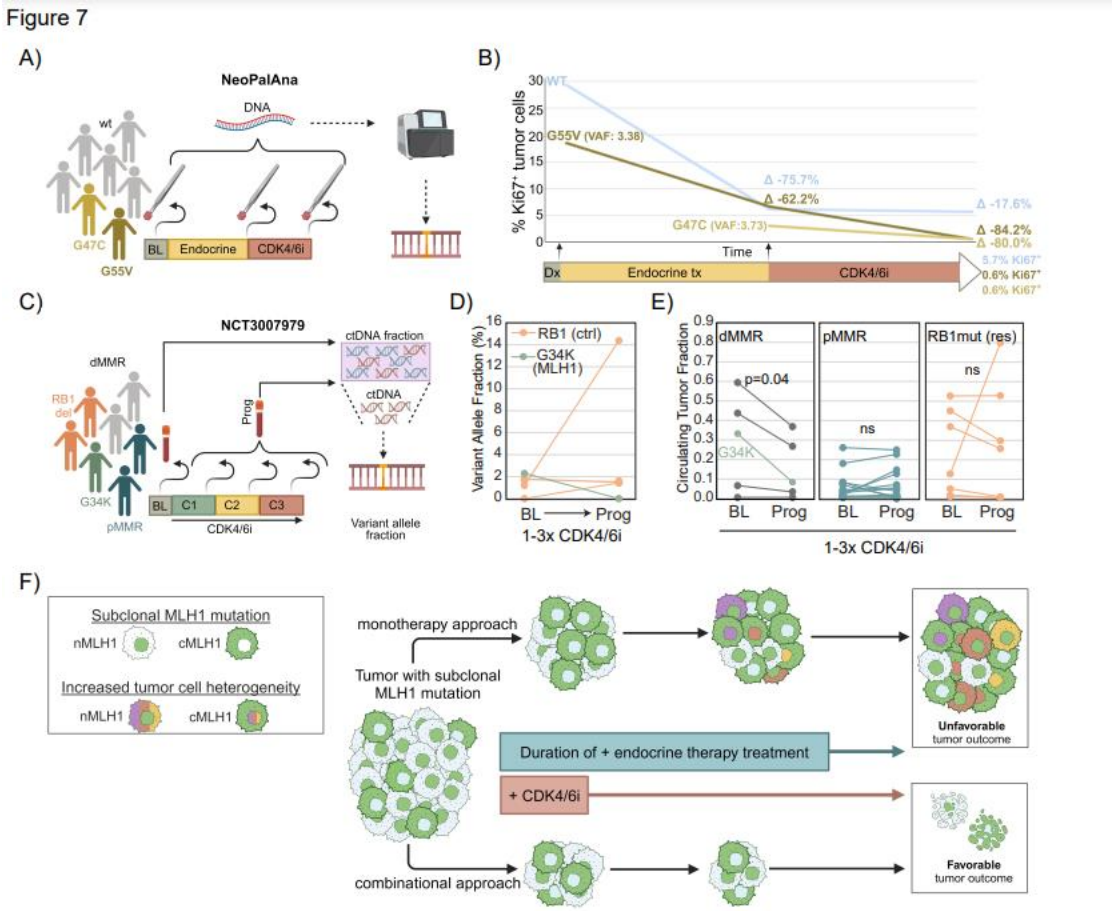

Figure 7: MLH1 mutations in patient tumors and CDK4/6 inhibitor response. (A) Schema of longitudinal clinical trial. In NeoPalAna whole exome sequencing was performed in patient biopsies at baseline, after endocrine therapy and after endocrine therapy in combination with palbociclib. (B) Line graph showing Ki67+ staining in WT patient tumors compared to G55V and G47C tumors after each round of treatment. (C) Schema for NCT3007979 trial where ctDNA was isolated from patients to evaluate genomic alterations, mutational signatures, and blood tumor mutational burden. Whole-genome sequencing was performed at baseline and serial timepoints to assess blood copy-number burden. (D) Line graph showing VAF % of Rb1 and G34K at baseline and after 3 cycles of CDK4/6 inhibitor treatment. (E) Line graph showing circulating tumor fraction in MMR deficient (dMMR), MMR proficient (pMMR) and Rb1 mutated patient. (F) Working model. Tumor cells carrying MLH1 mutations where MLH1 is expressed in the cytoplasm escape endocrine monotherapy which may result in increased tumor cell heterogeneity with an unfavorable outcome in these patients. These tumor cells will respond better when CDK4/6 inhibitors are given in combination with endocrine therapy in an adjuvant setting. t test was performed to determine all p values. * represent $p<0.05$. Abbreviations, Baseline (BL), CDK4/6 inhibitor (CDKi), Cycle 1,2,3 (C1,C2,C3), Circulating DNA

(ctDNA), Progression (Prog), Deficient for MMR (dMMR), Proficient for MMR (pMMR), Nuclear MLH1 (nMLH1), Cytoplasmic MLH1 (cMLH1), Not significant (ns).

we found a G34K mutation in the same ATPase domain of *MLH1.* This mutation decreases in VAF after 3 cycles of CDK4/6 inhibition from 2.5% to undetectable (Fig 7D). As control, we found that the VAF of RB1 deletion, a known driver of resistance to palbociclib, increases after exposure to treatment from 1% to 14% (Fig 7D). Patients were categorized as deficient or proficient for MMR based on high bTMB and microstatellite instability. Using this categorization, we found that the patient with the G34K variant, as well as other patients categorized as deficient in MMR showed significant decreased in total ctDNA load with repeated exposure to palbociclib in contrast to patients who were proficient for MMR or had RB1 variants associated with resistance to palbociclib (Fig 7E). Overall, these data suggest that sub-clonal populations bearing MLH1 mutations perturbing sub-celluar localization of the protein may serve as persister-like populations seeding resistance to standard endocrine therapy but proving highly susceptible to combinatorial treatment with CDK4/6 inhibitors (Fig 7F).

Discussion.

Although CDK4/6 inhibitors in the metastatic setting have demonstrated significant clinical benefit in ER+/HER2- patients, results from PALLAS, PENELOPE-B, monarchE and NATALEE trials, where the benefit of CDK4/6 inhibition was tested in the adjuvant setting in early-stage ER+/HER2- patients remain conflicting [22], [23], [24], [25], [26]. There is consensus within the cancer research community that the adjuvant use of CDK4/6 inhibitors, which would greatly benefit a subset of patients, is only achievable with the identification of predictive biomarkers that can be assessed at diagnosis [27], [28], [29], [30]. Currently, there are no specific predictive biomarkers for the adjuvant use of CDK4/6 inhibitors, and clinicians rely on more generic indicators of proliferation, such as high Ki67, to guide decision making on the administration of CDK4/6 inhibitors. However, the inaccuracy of Ki-

67 as a biomarker for administering CDK4/6 inhibitors to patients with ER+/HER2- breast cancer are widely acknowledged [31], [32].

The results presented here suggest that cytoplasmic localization of MLH1 could constitute a first-in-class predictive marker, assayable at diagnosis, for responsiveness to CDK4/6 inhibition in the subset of ER+/HER2− breast cancer patients most likely to be resistant to standard endocrine therapies. The role of MLH1 in breast cancer is not well-studied since breast cancer does not fall under the canonical Lynch syndrome spectrum of cancers that are triggered by the germline loss of mismatch repair genes [33]. However, we and other groups have shown a role for somatic MLH1 loss in inducing endocrine therapy resistance and poor outcomes in ER+/HER2- breast cancer patients that requires more investigation [7], [34]. Within this context, it is important to note that *MLH1* mutations are not common in ER+/HER2- breast cancer, occurring in 1-2% of patients. However, this may be due to the sub-clonal nature of *MLH1* mutations which can cause them to go clinically undetected. Conversely, the sub-clonal nature of these mutations supports a role for them in constituting persister cell pools that can resurface as treatment resistant recurrences many years after diagnosis and initial apparent therapeutic response [35], [36].

In the present study, we characterize the G55V mutation which clearly induces resistance to endocrine therapy. Most *MLH1* missense mutations have low allele frequency. Patients with the G55V mutation in the NeoPalAna trial had allele frequency of 3.38 and therefore showed significant inhibition of tumor burden after endocrine therapy for 28 days [37]. Nevertheless, in our sub-clonal *in vitro*, 3D as well as xenograft tumor assays G55V-expressing cells are only minimally responsive to all forms of endocrine intervention and could persist for extended periods in the host while the bulk of the tumor (wildtype for MLH1) shrinks in response to therapy. Conversely, administration of a CDK4/6 inhibitor in these experimental settings, while having little effect on the wildtype MLH1-expressing tumor bulk, is extremely effective in curbing the G55V-bearing population.

Therefore, our data supports the use of these *MLH1* mutations, even in sub-clonal populations, as predictive for combinatorial, adjuvant administration of endocrine therapy and CDK4/6 inhibitors.

The mechanism by which mutations such as G55V induce endocrine therapy resistance and responsiveness to CDK4/6 inhibition is likely through aberrant localization of MLH1 to the cytoplasm rather than the nucleus. Currently, subcellular localization of MLH1 is not assessed as part of routine clinical diagnostics for mismatch repair loss. However, multiple levels of orthogonal data presented here suggest that even in the presence of abundant MLH1 protein levels, aberrant cytoplasmic localization of the protein significantly decreases activation of Chk2 in response to endocrine therapy. Concordantly, adding a CHK2 activator (DIM) to cells with cytoplasmic MLH1, or inhibiting downstream effectors such as CDK4/6, rescues endocrine therapy responsiveness. Importantly, *CHEK2* germline variants specifically associate with increased incidence of ER+ tumors, suggesting the role of CHK2 in connecting ER to the cell cycle as highlighted in our investigation is fundamental to development of luminal tumors [38]. These data taken together provide the first evidence for considering cytoplasmic MLH1 as a first-in class biomarker that predicts cellular response to front-line CDK4/6 inhibition. The impact of this discovery could be substantial, given that cytoplasmic MLH1, caused by *MLH1* mutation as well as other non-mutational events, occurs in ~12% of ER+/HER2− breast cancer patients (~22,000 patients a year in the US alone). Given that immunohistochemistry-based staining for MLH1 is routinely used in the clinic for colorectal and endometrial cancer patients, it is feasible to co-opt this diagnostic to detect levels of subcellular MLH1 localization for the assessment of ER+/HER2− breast cancer patients [39], [40].

References:

[1] T. C. Brown and J. Jiricny, "Repair of base-base mismatches in simian and human cells," *Genome*, vol. 31, no. 2, pp. 578–583, 1989, doi: 10.1139/g89-107.

[2] A. Dal Buono, F. Gaiani, L. Poliani, C. Correale, and L. Laghi, "Defects in MMR Genes as a Seminal Example of Personalized Medicine: From Diagnosis to Therapy," *J. Pers. Med.*, vol. 11, no. 12, Art. no. 12, Dec. 2021, doi: 10.3390/jpm11121333.

[3] E. Vilar and S. B. Gruber, "Microsatellite instability in colorectal cancer—the stable evidence," *Nat. Rev. Clin. Oncol.*, vol. 7, no. 3, Art. no. 3, Mar. 2010, doi: 10.1038/nrclinonc.2009.237.

[4] M. Hewish, C. J. Lord, S. A. Martin, D. Cunningham, and A. Ashworth, "Mismatch repair deficient colorectal cancer in the era of personalized treatment," *Nat. Rev. Clin. Oncol.*, vol. 7, no. 4, Art. no. 4, Apr. 2010, doi: 10.1038/nrclinonc.2010.18.

[5] E. Sajjadi *et al.*, "Mismatch repair-deficient hormone receptor-positive breast cancers: Biology and pathological characterization," *Cancer Cell Int.*, vol. 21, no. 1, p. 266, May 2021, doi: 10.1186/s12935-021-01976-y.

[6] N. Fusco *et al.*, "Mismatch Repair Protein Loss as a Prognostic and Predictive Biomarker in Breast Cancers Regardless of Microsatellite Instability," *JNCI Cancer Spectr.*, vol. 2, no. 4, p. pky056, Dec. 2018, doi: 10.1093/jncics/pky056.

[7] S. Haricharan *et al.*, "Loss of MutL Disrupts CHK2-Dependent Cell-Cycle Control through CDK4/6 to Promote Intrinsic Endocrine Therapy Resistance in Primary Breast Cancer," *Cancer Discov.*, vol. 7, no. 10, pp. 1168–1183, Oct. 2017, doi: 10.1158/2159-8290.CD-16-1179.

[8] F. Chen *et al.*, "Single-cell transcriptomic heterogeneity in invasive ductal and lobular breast cancer cells," *Cancer Res.*, vol. 81, no. 2, pp. 268–281, Jan. 2021, doi: 10.1158/0008-5472.CAN-20-0696.

[9] N. McGranahan and C. Swanton, "Clonal Heterogeneity and Tumor Evolution: Past, Present, and the Future," *Cell*, vol. 168, no. 4, pp. 613–628, Feb. 2017, doi: 10.1016/j.cell.2017.01.018.

[10] A. Pribluda, C. C. de la Cruz, and E. L. Jackson, "Intratumoral Heterogeneity: From Diversity Comes Resistance," *Clin. Cancer Res. Off. J. Am. Assoc. Cancer Res.*, vol. 21, no. 13, pp. 2916–2923, Jul. 2015, doi: 10.1158/1078-0432.CCR-14-1213.

[11] Y. Pu *et al.*, "Drug-tolerant persister cells in cancer: the cutting edges and future directions," *Nat. Rev. Clin. Oncol.*, vol. 20, no. 11, pp. 799–813, Nov. 2023, doi: 10.1038/s41571-023-00815-5.

[12] P. K. Dhanyamraju, T. D. Schell, S. Amin, and G. P. Robertson, "Drug-Tolerant Persister Cells in Cancer Therapy Resistance," *Cancer Res.*, vol. 82, no. 14, pp. 2503–2514, Jul. 2022, doi: 10.1158/0008-5472.CAN-21-3844.

[13] S. Haricharan, M. N. Bainbridge, P. Scheet, and P. H. Brown, "Somatic mutation load of estrogen receptor-positive breast tumors predicts overall survival: an analysis of genome sequence data," *Breast Cancer Res. Treat.*, vol. 146, no. 1, pp. 211–220, Jul. 2014, doi: 10.1007/s10549-014-2991-x.

[14] M. W. Fittall and P. Van Loo, "Translating insights into tumor evolution to clinical practice: promises and challenges," *Genome Med.*, vol. 11, p. 20, Mar. 2019, doi: 10.1186/s13073-019-0632-z.
[15] L. R. Yates *et al.*, "Genomic Evolution of Breast Cancer Metastasis and Relapse," *Cancer Cell*, vol. 32, no. 2, pp. 169-184.e7, Aug. 2017, doi: 10.1016/j.ccell.2017.07.005.
[16] A. B. Hanker, D. R. Sudhan, and C. L. Arteaga, "Overcoming Endocrine Resistance in Breast Cancer," *Cancer Cell*, vol. 37, no. 4, pp. 496–513, Apr. 2020, doi: 10.1016/j.ccell.2020.03.009.
[17] P. Razavi *et al.*, "The Genomic Landscape of Endocrine-Resistant Advanced Breast Cancers," *Cancer Cell*, vol. 34, no. 3, pp. 427-438.e6, Sep. 2018, doi: 10.1016/j.ccell.2018.08.008.
[18] W. Shao and M. Brown, "Advances in estrogen receptor biology: prospects for improvements in targeted breast cancer therapy," *Breast Cancer Res. BCR*, vol. 6, no. 1, pp. 39–52, 2004, doi: 10.1186/bcr742.
[19] J. T. Lei, M. Anurag, S. Haricharan, X. Gou, and M. J. Ellis, "Endocrine therapy resistance: new insights," *Breast Edinb. Scotl.*, vol. 48 Suppl 1, no. Suppl 1, pp. S26–S30, Nov. 2019, doi: 10.1016/S0960-9776(19)31118-X.
[20] B. O'Leary, R. S. Finn, and N. C. Turner, "Treating cancer with selective CDK4/6 inhibitors," *Nat. Rev. Clin. Oncol.*, vol. 13, no. 7, pp. 417–430, Jul. 2016, doi: 10.1038/nrclinonc.2016.26.
[21] "Personalized Medicine: Identifying the Appropriate Patient Through Biomarkers in Oncology," *Pharm. Ther.*, vol. 36, no. 7 Suppl 1, pp. 3–10, Jul. 2011.
[22] E. L. Mayer *et al.*, "Palbociclib with adjuvant endocrine therapy in early breast cancer (PALLAS): interim analysis of a multicentre, open-label, randomised, phase 3 study," *Lancet Oncol.*, vol. 22, no. 2, pp. 212–222, Feb. 2021, doi: 10.1016/S1470-2045(20)30642-2.
[23] S. Loibl *et al.*, "Palbociclib for Residual High-Risk Invasive HR-Positive and HER2-Negative Early Breast Cancer—The Penelope-B Trial," *J. Clin. Oncol.*, vol. 39, no. 14, pp. 1518–1530, May 2021, doi: 10.1200/JCO.20.03639.
[24] S. R. D. Johnston *et al.*, "Abemaciclib plus endocrine therapy for hormone receptor-positive, HER2-negative, node-positive, high-risk early breast cancer (monarchE): results from a preplanned interim analysis of a randomised, open-label, phase 3 trial," *Lancet Oncol.*, vol. 24, no. 1, pp. 77–90, Jan. 2023, doi: 10.1016/S1470-2045(22)00694-5.
[25] D. J. Slamon *et al.*, "Ribociclib and endocrine therapy as adjuvant treatment in patients with HR+/HER2- early breast cancer: Primary results from the phase III NATALEE trial.," *J. Clin. Oncol.*, vol. 41, no. 17_suppl, pp. LBA500–LBA500, Jun. 2023, doi: 10.1200/JCO.2023.41.17_suppl.LBA500.
[26] L. Morrison, S. Loibl, and N. C. Turner, "The CDK4/6 inhibitor revolution — a game-changing era for breast cancer treatment," *Nat. Rev. Clin. Oncol.*, vol. 21, no. 2, Art. no. 2, Feb. 2024, doi: 10.1038/s41571-023-00840-4.

[27] S. F. Schoninger and S. W. Blain, “The ongoing search for biomarkers of CDK4/6 inhibitor responsiveness in Breast Cancer,” *Mol. Cancer Ther.*, vol. 19, no. 1, pp. 3–12, Jan. 2020, doi: 10.1158/1535-7163.MCT-19-0253.
[28] U. S. Asghar, R. Kanani, R. Roylance, and S. Mittnacht, “Systematic Review of Molecular Biomarkers Predictive of Resistance to CDK4/6 Inhibition in Metastatic Breast Cancer,” *JCO Precis. Oncol.*, no. 6, p. e2100002, Dec. 2022, doi: 10.1200/PO.21.00002.
[29] T. B. V. Bui, B. M. T. Burgering, A. Goga, H. S. Rugo, and L. J. van ‘t Veer, “Biomarkers for Cyclin-Dependent Kinase 4/6 Inhibitors in the Treatment of Hormone Receptor-Positive/Human Epidermal Growth Factor Receptor 2-Negative Advanced/Metastatic Breast Cancer: Translation to Clinical Practice,” *JCO Precis. Oncol.*, no. 6, p. e2100473, Dec. 2022, doi: 10.1200/PO.21.00473.
[30] M. Anurag, S. Haricharan, and M. J. Ellis, “CDK4/6 Inhibitor Biomarker Research: Are We Barking Up the Wrong Tree?,” *Clin. Cancer Res. Off. J. Am. Assoc. Cancer Res.*, vol. 26, no. 1, pp. 3–5, Jan. 2020, doi: 10.1158/1078-0432.CCR-19-3119.
[31] C. Selli, J. M. Dixon, and A. H. Sims, “Accurate prediction of response to endocrine therapy in breast cancer patients: current and future biomarkers,” *Breast Cancer Res.*, vol. 18, no. 1, p. 118, Dec. 2016, doi: 10.1186/s13058-016-0779-0.
[32] N. Portman, S. Alexandrou, E. Carson, S. Wang, E. Lim, and C. E. Caldon, “Overcoming CDK4/6 inhibitor resistance in ER-positive breast cancer,” *Endocr. Relat. Cancer*, vol. 26, no. 1, pp. R15–R30, Jan. 2019, doi: 10.1530/ERC-18-0317.
[33] J. M. Ford, “Is breast cancer a part of Lynch syndrome?,” *Breast Cancer Res. BCR*, vol. 14, no. 4, p. 110, 2012, doi: 10.1186/bcr3241.
[34] A. S. Cheng *et al.*, “Mismatch repair protein loss in breast cancer: clinicopathological associations in a large British Columbia cohort,” *Breast Cancer Res. Treat.*, vol. 179, no. 1, pp. 3–10, Jan. 2020, doi: 10.1007/s10549-019-05438-y.
[35] H. F. Cabanos and A. N. Hata, “Emerging Insights into Targeted Therapy-Tolerant Persister Cells in Cancer,” *Cancers*, vol. 13, no. 11, p. 2666, May 2021, doi: 10.3390/cancers13112666.
[36] G. De Conti, M. H. Dias, and R. Bernards, “Fighting Drug Resistance through the Targeting of Drug-Tolerant Persister Cells,” *Cancers*, vol. 13, no. 5, Art. no. 5, Jan. 2021, doi: 10.3390/cancers13051118.
[37] C. X. Ma *et al.*, “NeoPalAna: Neoadjuvant Palbociclib, a Cyclin-Dependent Kinase 4/6 Inhibitor, and Anastrozole for Clinical Stage 2 or 3 Estrogen Receptor-Positive Breast Cancer,” *Clin. Cancer Res. Off. J. Am. Assoc. Cancer Res.*, vol. 23, no. 15, pp. 4055–4065, Aug. 2017, doi: 10.1158/1078-0432.CCR-16-3206.
[38] E. Oropeza *et al.*, “Molecular portraits of cell cycle checkpoint kinases in cancer evolution, progression, and treatment responsiveness,” *Sci. Adv.*, vol. 9, no. 26, p. eadf2860, Jun. 2023, doi: 10.1126/sciadv.adf2860.

[39] T. A. P. Staff, “Companion Diagnostic to Identify Patients With Endometrial Cancer Eligible for Pembrolizumab Therapy Approved by the FDA - The ASCO Post.” Accessed: Feb. 12, 2024. [Online]. Available: https://ascopost.com/issues/september-10-2022/companion-diagnostic-to-identify-patients-with-endometrial-cancer-eligible-for-pembrolizumab-therapy-approved-by-the-fda/

[40] P. Vikas *et al.*, “Mismatch Repair and Microsatellite Instability Testing for Immune Checkpoint Inhibitor Therapy: ASCO Endorsement of College of American Pathologists Guideline,” *J. Clin. Oncol.*, vol. 41, no. 10, pp. 1943–1948, Apr. 2023, doi: 10.1200/JCO.22.02462.